JOURNAL OF SOLID STATE CHEMISTRY 92, 301–311 (1991)

Tetragonal and Cubic Crystal Structures of Some Binary and Ternary Metal Dicarbides in the Series Ce–Er, Ce–Lu, U–La, and U–Ce

D. W. JONES,* I. J. McCOLM,† AND J. YERKESS*

*Departments of *Chemistry and Chemical Technology and †Industrial Technology, University of Bradford, Bradford, West Yorkshire, BD7 1DP, United Kingdom*

Received October 5, 1989; in revised form January 16, 1991

The binary dicarbides LaC_2 and ErC_2 (tetragonal, space group $I4/mmm$, $Z = 2$) and the ternary dicarbides $Ce_{0.50}Er_{0.50}C_2$, $Ce_{0.75}Lu_{0.25}C_2$, $Ce_{0.50}Lu_{0.50}C_2$, $Ce_{0.25}Lu_{0.75}C_2$, $U_{0.75}La_{0.25}C_2$, $U_{0.50}La_{0.50}C_2$, $U_{0.25}La_{0.75}C_2$, $U_{0.75}Ce_{0.25}C_2$, $U_{0.50}Ce_{0.50}C_2$, and $U_{0.25}Ce_{0.75}C_2$ (cubic, space group $Fm3m$, $Z = 4$) have been prepared by arc melting, and their metal compositions confirmed by point energy dispersion X-ray analysis by scanning electron microscopy. Their neutron powder diffraction patterns have been recorded at room temperature and, for the three Ce–Lu compounds, also at 4.2 K (at which temperature the cubic structure is retained). For LaC_2 and ErC_2, mild hydrolysis indicates the presence of acetylide units, and Rietveld profile analysis of the neutron data has enabled the unit-cell dimensions (a, c = 3.937(1), 6.579(2) Å and 3.622(1), 6.106(1) Å, respectively) and the C–C bond lengths (1.284(6) and 1.275(3) Å, respectively) to be refined. For the ternary compounds (some of which contain two face-centered cubic (f.c.c.) phases), the distinctive martensitic microstructure is absent from micrographs, and the limited neutron integrated intensity data appear to be consistent with f.c.c. structures having either static or rotating C–C groups.

1. Introduction

The body-centered tetragonal (b.c.t.) dicarbides of lanthanide and actinide metals are known (*1*, *2*) to transform to a face-centered cubic (f.c.c.) phase at temperatures of 1000–1900 K, so that structural studies of the cubic phase have been difficult to carry out. Dicarbides of the periodic group II elements transform to the cubic phase at much lower temperatures (400–700 K) and should, therefore, be more easily examined; since, however, they are more difficult to prepare as pure phases than the lanthanide and actinide dicarbides, few detailed studies have been made. Early neutron diffraction data for the cubic phases of calcium (*3*), lanthanum (*4*), uranium (*5*), and thorium (*6*) dicarbides are equally consistent with two structure models:

(1) Static, with metal atoms at 0,0,1/2 and C–C groups centered on 0,0,0 but oriented randomly along the [111] directions so that the carbon atoms occupy positions x,x,x with an occupation factor of one-fourth.

(2) Dynamic, with the C–C groups freely rotating over the surface of a sphere centered on 0,0,0.

The structure of the high-temperature phase is of some interest because the cu-

0022-4596/91 $3.00

bic–tetragonal transformation shows many of the characteristics of a type known as brittle-martensitic. Such changes have considerable potential for improving the toughness of ceramic systems that contain partially stabilized high-temperature polymorphs; hence the interest in the tetragonal–monoclinic transformation in ZrO_2 (*7*).

In a martensitic phase, nucleation is critical; once nucleated, the transformation proceeds at the velocity of sound with concerted reorientation and no diffusion. A strain-energy component allows some control of the nucleation stage so that the transformation temperature can be lowered. For dicarbides, this strain effect has been demonstrated and measured (*8*) by substitution of the small cations by larger ones in the solute dicarbide (*1, 2*). In some ternary dicarbide systems, such as Ce–Er and Ce–Lu, the transformation temperature can be depressed to below room temperature so that samples of the cubic phase become more readily available for study. In other cases, such as U–La and U–Ce, the strain energy, allied to a rapid-cooling stage, leads either to a single phase or to two cubic phases depending upon the composition.

In this paper we report room-temperature and 4.2 K neutron powder diffraction studies of some cubic ternary dicarbides in the series Ce–Er, Ce–Lu, U–La, and U–Ce (pairs with sufficiently different ionic radii to depress the nucleation of the tetragonal phase to ambient temperature) and Rietveld line-profile refinements for tetragonal binary dicarbides LaC_2 and ErC_2 (for comparison with similar refinements for CeC_2 and UC_2 (*9, 10*)), together with some X-ray diffraction, hydrolytic and metallographic studies. The tetragonal dicarbides have been reexamined in order to provide further insight into the bond model for the dicarbides. At present, dicarbides are modelled as metal cations, M^{n+}, and dicarbide anions, C_2^{2-}, with a delocalized band formed by interactions between $p\pi^*$ antibonding orbitals from the anions and *s*, *d*, and *f* orbitals from the cations; electrons from the cations occupy the antibonding levels of the anions. Thus, while M^{n+}–C_2^{2-} bond lengths would be expected to decrease as *n* increases from group II to the actinides, the C–C distances should increase. For lanthanides, where $n = 3$, changes in the C–C distance might be linked to *f*-orbital participation in the bonding. Such participation is thought to be high for the light lanthanides but not for the heavy ones (*11*); LaC_2 and ErC_2, respectively, provide examples for comparison.

2. Experimental

2.1 Sample Preparation

The dicarbides were prepared by direct high-temperature synthesis from stoichiometric quantities of the constituent elements in an argon arc furnace, with about 3% excess carbon to ensure removal of any oxide in the metals. The starting materials were in the form of coarse grains or lumps (rather than powder) in order to eliminate losses due to removal of finely divided powder from the reaction zone by the pressure of the arc flame (*12, 13*). The metals (minimum purity 99.9%) were supplied as arc-melted rods by Koch-Light Limited (for the uranium) and Rare Earth Products Limited (for the lanthanides). The carbon was in the form of Specpure graphite rods. In each preparative run, the bead of material was turned and remelted three times; beads were discarded if the weight loss exceeded 0.5%.

Each run yielded a 0.5- to 1.0-g pellet of dicarbide which was pulverized in a percussion mortar in a dry argon atmosphere. The products of about 10 preparative runs were then combined to give about 5–10 g of material for the neutron diffraction measurements.

Total carbon contents were estimated from the barium carbonate precipitated after the weighed sample had been burned in oxygen on a platinum catalyst to oxidize any

TABLE I

DISTRIBUTION OF PERCENTAGES OF GASEOUS PRODUCTS FROM MILD HYDROLYSIS OF SOME DICARBIDES

Product	LaC_2 tetragonal	ErC_2 tetragonal	$Ce_{0.5}Er_{0.5}C_2$ cubic
CH_4	0.24	6.32	0.03
C_2H_6	6.77	4.84	2.7
C_2H_4	2.54	10.3	2.7
C_2H_2	89.5	78.5	94.6
C_3H_8	0.14	0.02	0.0
Total C_2	98.9	93.7	100.0

carbon monoxide while suspended over barium nitrate solution in a sealed pyrex system. Free or unreacted carbon was determined by dissolving a weighed sample in dilute hydrochloric acid and collecting the residual solid on a weighed sintered glass disk. Waxy hydrocarbons in the residue, which were insoluble in dilute hydrochloric acid, were removed by washing with acetone and benzene to enable free carbon to be determined by weighing; it was typically less than 0.5%.

2.2 Hydrolytic and Structural Examination

X-ray patterns (from an Expectron XDC 700 Hägg-Guinier focusing camera with Cr$K\alpha$ radiation) of carefully dried powders in sealed capillaries revealed some strain broadening for the cubic ternary compounds. For $Ce_{0.50}Er_{0.50}C_2$, heating at 800°C for 20 days or at 1500°C for 23 hr did not significantly alter the X-ray-determined cell dimensions from the arc-cast value of 5.65 Å derived from reflections 111(medium strong), 200(strong), 220(medium strong), 222(medium), 400(weak), 331(strong), 420(medium strong), 422(strong).

Analysis of the hydrocarbon products of mild hydrolysis (*13*) showed (Table I) the presence of paired carbon units in both the tetragonal and the cubic phases. Surface reactions of C_2H_2 gave rise to small but detectable amounts of C_3H_8 and higher hydrocarbons from LaC_2 and ErC_2 but not from the ternary compounds.

The reliability of the compositional formulae, derived from weighings, was reinforced by *in situ* energy dispersion X-ray (EDX) phase analysis with an ISI Super IIIA scanning electron microscope (SEM). The micrograph of $U_{0.50}La_{0.50}C_2$ (Fig. 1a) displays an array of light areas (U-rich) and dark areas (La-rich) carrying oxide scale (individual areas are smaller than the beam size). The overall EDX analysis across the grain corresponds to $U_{0.50}La_{0.50}$ stoichiometry, just as from weighings. Point measurements for metal content on the light areas yielded $U_{0.76}La_{0.24}C_2$ as the La-saturated UC_2 cubic solid solution. For the dark areas, higher oxidation rates contributed to some variation but all measurements showed La > U with a maximum of $U_{0.41}La_{0.59}$. The other end of the miscibility gap is expected to be closer to a composition of $U_{0.30}La_{0.70}C_2$.

For $Ce_{0.75}Lu_{0.25}C_2$ on the other hand, despite rapid surface oxidation, SEM micrographs indicated an even distribution of the two metals in a single phase. From several EDX spot analyses, the average composition corresponding to $Ce_{0.77}Lu_{0.25}C_2$ is almost identical to that from the mass balance composition. For $Ce_{0.50}Er_{0.50}C_2$, which also showed oxygen reactivity after surface polishing, an unsegregated single-phase uniform distribution of Ce and Er was apparent throughout, in accord with the Hägg–Guinier photographs.

For comparison with the cubic ternary dicarbides discussed here, Fig. 1b shows an optical micrograph in polarized light of a b.c.t. solid solution, $Pr_{0.70}Ho_{0.30}C_2$. Inclined striations characteristic of martensitic twins are evident. The complete absence of this distinctive microstructure (and also of significant amounts of free carbon) in these untransformed cubic solid solutions is evi-

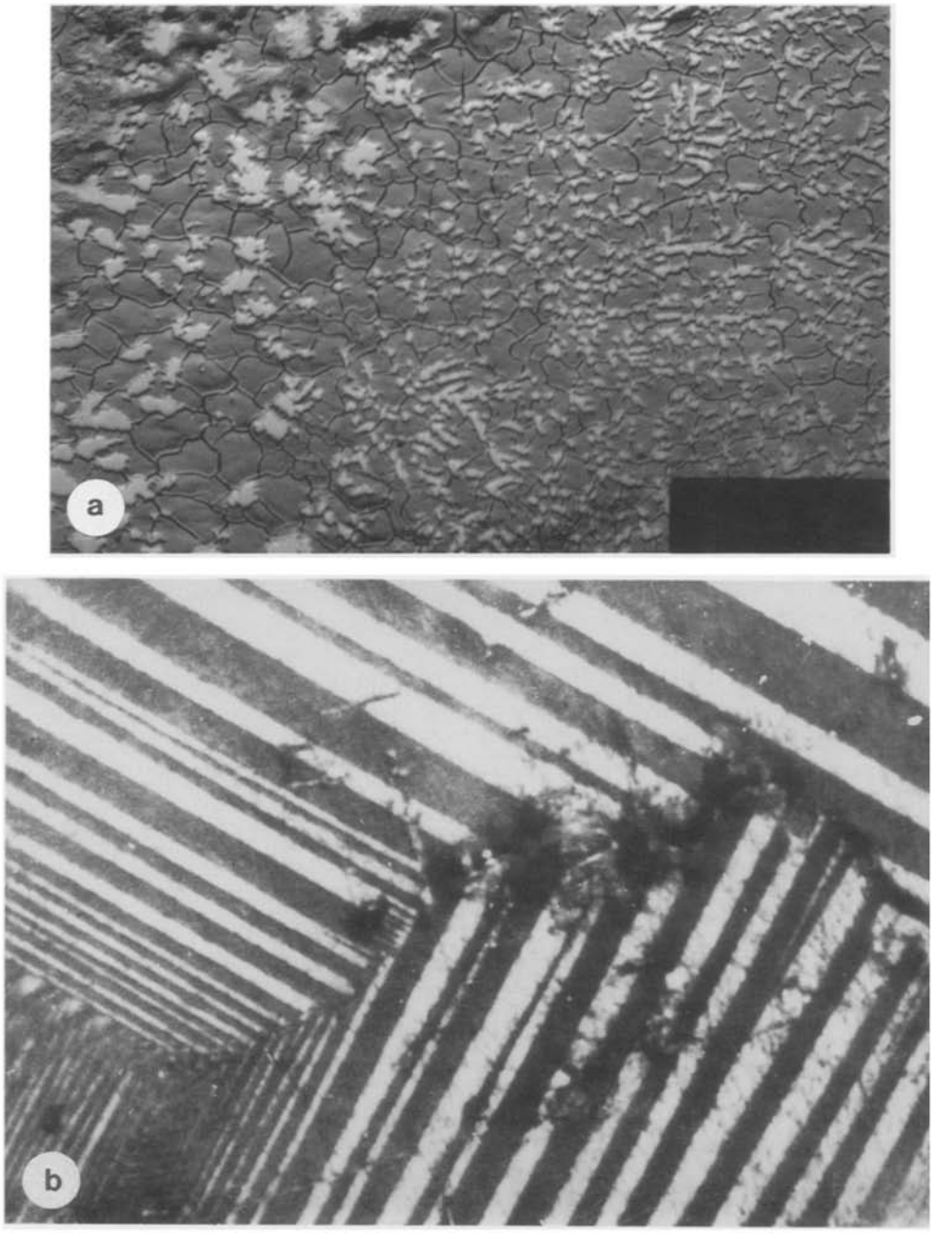

FIG. 1. Micrographs of arc-cast ternary dicarbide solid solutions: (a) SEM micrograph of $U_{0.50}La_{0.50}C_2$ $\times 150$ showing distributions of light (U-rich) and dark (La-rich) phases in two-phase mixture. (b) Optical micrograph of $Pr_{0.70}Ho_{0.30}C_2$ $\times 380$ in polarized light to illustrate striations characteristic of martensitic twins in tetragonal lanthanide dicarbide structure.

TABLE II

INSTRUMENTAL DETAILS FOR COLLECTION OF NEUTRON DIFFRACTION DATA

Compounds	LaC_2	$U_{0.75}La_{0.25}C_2$ $U_{0.75}Ce_{0.25}C_2$ ErC_2	$U_{0.50}La_{0.50}C_2$ $U_{0.25}La_{0.75}C_2$ $U_{0.50}Ce_{0.50}C_2$ $U_{0.25}Ce_{0.75}C_2$	$Ce_{0.50}Er_{0.50}C_2$ $Ce_{0.75}Lu_{0.25}C_2$ $Ce_{0.50}Lu_{0.50}C_2$ $Ce_{0.25}Lu_{0.75}C_2$
Reactor	DIDO AERE	HFR, ILL, Grenoble	DIDO AERE	HERALD AWRE
Diffractometer	CURRAN[a] (5 counters at 10° intervals)	D2	BADGER	VANESSA[b] (8 counters at 15° intervals)
Wavelength (Å)	1.378	1.119	1.125	1.100
2θ range (deg)	5 to 57 and 55 to 107	10 to 120	10 to 75	−10 to +110
Step increment (2θ)	0.1°	0.1°	0.1°	0.1°
Counting time point^{-1} (min)	3.0	0.7	1.0	14.0
Recording time per sample (hr)	13	12	18	35

[a] The complete run on CURRAN was made in two parts. In part 1, counter one covered the range 2θ = 5–17°; counter two, 2θ = 15–27°; and so on to cover the range 5–57° in all (with a 2° overlap between consecutive counters). In part 2, counter one covered the range 55–107° so that the overall range was 55–107°, again with a 2° overlap. Corrections for differing counter efficiencies were applied.

[b] A 15° scan on VANESSA covered a 2θ range of 120°. Corrections for differing counter efficiencies were applied.

dence of their failure to nucleate tetragonal material on cooling. No tetragonal ternary phases were detected in the present series, not even over regions as small as the 10 μm over which the polarized light microscopy could detect twinning microstructure.

2.3 Neutron Diffraction Data

Neutron diffraction patterns of the samples, contained in thin-walled 0.5 cm diameter cylindrical vanadium cans, were recorded (Table II) on four diffractometers at three different reactor sites: (a) the High Flux Reactor (HFR) at the Institut Laue-Langevin, Grenoble, (b) the DIDO Reactor at AERE, Harwell, and (c) the HERALD Reactor at AWRE, Aldermaston. Neutron wavelengths were determined from powder diffraction patterns on annealed nickel powder. Diffraction patterns for every sample were recorded at room temperature; those for the three Ce–Lu compounds were also recorded at 4.2 K.

Neutron scattering amplitudes used in subsequent data analysis were (14): b_C = 6.65 fm; b_{La} = 8.3 fm; b_{Ce} = 4.8 fm; b_{Er} = 7.9 fm; b_{Lu} = 7.3 fm; b_U = 8.5 fm.

2.4 Structure Refinement

2.4.1 LaC_2 and ErC_2. The starting point for the refinements was the structure established by Spedding *et al.* (*15*) by X-ray powder diffraction, and confirmed by Atoji (*16, 17*) by refinement of neutron-diffraction powder peak intensities. The profile refinements (*18, 19*) followed a similar least-squares minimization procedure to that described previously (*9, 10, 20*) with 11 crystal-structural and instrumental parameters as variables.

Initial values for the structural parameters were:

TABLE III

RESULTS OF NEUTRON POWDER PROFILE REFINEMENTS FOR LaC_2 AND ErC_2

	LaC_2	ErC_2
a	3.937(1)	3.622(1)
c	6.580(2)	6.106(1)
z_c	0.4024(5)	0.3956(3)
B(M)	0.6(1)	0.18(5)
B(C)	0.4(1)	0.54(5)
μ	0.104	2.50
ΔB	0.002	0.21
R_p	0.166	0.106
R_{wp}	0.206	0.109
R_e	0.075	0.071
C–C	1.284(6)	1.275(3)
M–C	2.648(3)	2.416(2)

Note. Unit-cell dimensions a and c (Å); fractional coordinates of carbon atom z_c; thermal parameters B (Å^2); absorption coefficients μ (cm^{-1}); absorption corrections ΔB to B; unweighted (R_p), weighted (R_{wp}), and expected (R_e) agreement factors; C–C and M–C bond lengths (Å)(ESDs of least significant figures in parentheses)

(1) For LaC_2, a = 3.934 Å, c = 6.572 Å; for ErC_2, a = 3.620 Å, c = 6.094 Å (15).

(2) B = 0.5 Å^2 for both metal and carbon atoms in both structures.

(3) For LaC_2, z_c = 0.4009 (*16*); for ErC_2, z_c = 0.3943 (*17*).

Initial values for the instrumental parameters were determined as described previously (*9, 10, 20*). For both structures, the refinement converged (final results in Table III) in less than 10 cycles with final parameter shifts less than one-hundredth of the estimated standard deviation. No significant improvement or change in parameters resulted either from the introduction of anisotropic thermal parameters or from the recalculation of the profiles from the refined unit-cell and instrumental parameters (*21*).

The refined values of the instrumental parameters and the final agreement indices were similar to those obtained for other data from the same diffractometers (*10, 20, 22*). The poorer agreement for LaC_2 is probably due to poorer counting statistics and possible errors in the corrections for relative counter efficiencies on the multicounter diffractometer.

There were significant correlations between shifts for parameters within each of the following groups: (1) the isotropic thermal parameters (coefficients up to 0.8); (2) the peak-width parameters (coefficients greater than 0.9); (3) unit cell, zeropoint, and asymmetry parameters (coefficients from 0.4 to 0.9).

Scale factor shifts were correlated (coefficients up to 0.4) with the thermal parameter shifts, but z_c was not strongly correlated with any other parameter.

Figures 2 and 3 show the observed, calculated, and discrepancy profiles for the two structures. Lists of observed and calculated intensities have been deposited.[1]

The Hewat (*23*) absorption correction, ΔB, to the thermal parameters is significant for ErC_2 but not for LaC_2 (coefficients μ in Table III calculated from mass absorption coefficients: La, 0.023; Er, 0.36; C, 0.00015 cm^{2}g^{-1}). Thermal vibration corrections to bond lengths (which would tend to increase the apparent lengths of the C–C bonds) were not applied, since none of the usual models (*24*) seemed appropriate.

2.4.2 Cubic dicarbides. The neutron diffraction pattern of $U_{0.75}La_{0.25}C_2$, which showed only three strong peaks and a series of weaker ones, could be indexed as a mixture of two f.c.c. phases. For $U_{0.75}Ce_{0.25}C_2$

[1] See NAPS document No. 04858 for 6 pages of supplementary materials from ASIS/NAPS, Microfiche Publications, P.O. Box 3513, Grand Central Station, New York, NY 10163. Remit in advance $4.00 for microfiche copy or for photocopy, $7.75 up to 20 pages plus $0.30 for each additional page. All orders must be prepaid. Institutions and organizations may order by purchase order. However, there is a billing and handling charge for this service of $15. Foreign orders add $4.50 for postage and handling, for the first 20 pages, and $1.00 for additional 10 pages of material. Remit $1.50 for postage of any microfiche orders.

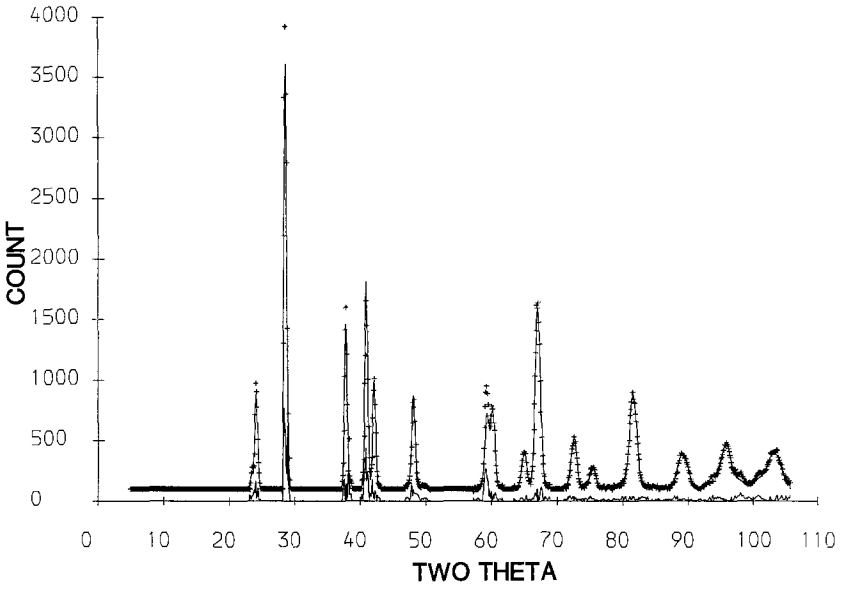

FIG. 2. Neutron powder-diffraction diagram for LaC_2: solid line, calculated profile; crosses, experimental intensities; differences between these are shown in the bottom line.

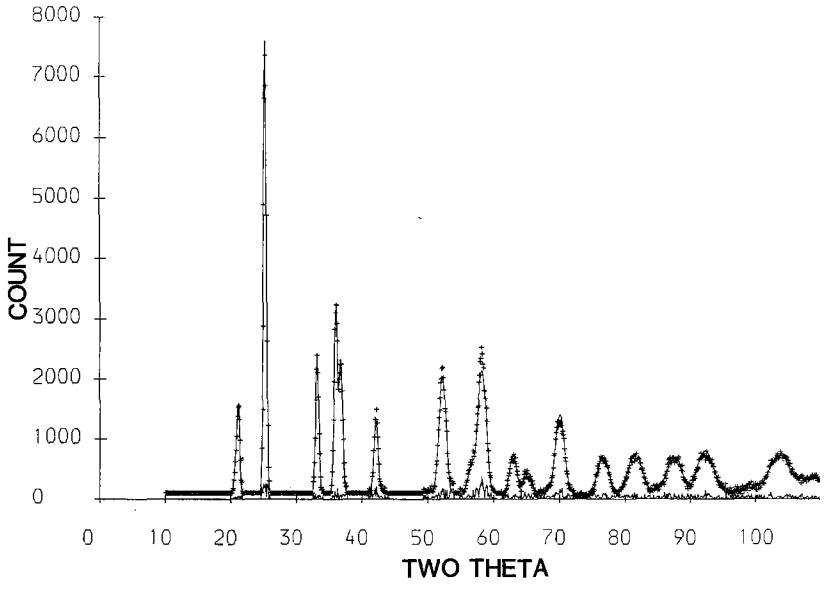

FIG. 3. Neutron powder-diffraction diagram for ErC_2: solid line, calculated profile; crosses, experimental intensities; differences between these are shown in the bottom line.

TABLE IV

UNIT-CELL PARAMETERS (Å) FOR CUBIC DICARBIDES DERIVED FROM NEUTRON DIFFRACTION POWDER PATTERNS

$Ce_{0.50}Er_{0.50}C_2$[a]	5.70(2)
$Ce_{0.75}Lu_{0.25}C_2$	5.75(1)
$Ce_{0.50}Lu_{0.50}C_2$	5.67(1)
$Ce_{0.25}Lu_{0.75}C_2$	5.55(1)
$Ce_{0.75}Lu_{0.25}C_2$ (4.2 K)	5.73(1)
$Ce_{0.50}Lu_{0.50}C_2$ (4.2 K)	5.90(3)
$Ce_{0.25}Lu_{0.75}C_2$ (4.2 K)	5.51(1)
$U_{0.75}La_{0.25}C_2$[b]	5.03(8)
	5.48(2)
$U_{0.50}La_{0.50}C_2$	5.52(2)
$U_{0.25}La_{0.75}C_2$	5.54(1)
$U_{0.75}Ce_{0.25}C_2$[b]	5.06(3)
	5.47(2)
$U_{0.50}Ce_{0.50}C_2$	5.34(1)
$U_{0.25}Ce_{0.75}C_2$	5.45(1)

Note. Measurements are at room temperature unless otherwise stated.

[a] 5.65 Å from X-ray powder data.

[b] These powder patterns were indexed on the basis of two f.c.c. lattices.

the stronger peaks could be indexed as a mixture of two f.c.c. phases, while most of the very weak peaks could be ascribed to unreacted graphite. With so few peaks, some overlapped, only the unit-cell parameters (Table IV) were derived (without any attempt to determine the structure).

Although the remaining diffraction patterns were all indicative of single-phase f.c.c. structures, the higher-angle peaks were broadened and overlapped. Unit-cell parameters (Table IV) were derived from the resolved peaks, but least-squares structure refinement (based on either profile or integrated intensities) was judged impracticable in view of the paucity of the data. Calculated structure factors (for comparison with observed values derived from integrated intensities) were therefore computed for a number of trial structures, based on both the static and the dynamic models, assuming random distribution of the metal atoms, with the x-coordinate of the carbon atom varying from 0.040 to 0.100 (corresponding to C–C bond lengths in the range 0.76 to 1.91 Å for a unit cell length of 5.50 Å) in increments of 0.001, and an overall isotropic thermal parameter varying from 0.02 Å^2 to 9.86 Å^2 in increments of 0.04 Å^2.

Calculated structure factors for the dynamic model were computed from the formula (*25*):

$$|F| = 4b_M \pm (8b_C \sin x/x),$$

where $x = 4\pi r \sin \Theta/\lambda$, r = radius of rotating group, b_M = weighted mean neutron scattering amplitude of the two metal atoms.

An agreement factor R was calculated for each of the x-coordinate/thermal parameter values, for each of the two structure models, to determine the parameter values which gave the best fit. The structure factor lists (Table V) for the best-fit parameters show agreement indices R based on the five reflections 111, 200, 220, 311, and 222 (four reflections only for $Ce_{0.75}Lu_{0.25}C_2$ and $Ce_{0.50}Lu_{0.50}C_2$ at 4.2 K where the 220 reflection could not be measured); in all cases, the 311 reflection was too weak to be observed and was assigned a zero intensity.

The structural parameters are shown in Table VI. The z_c parameters are probably accurate to about ±0.001 and the thermal parameters to about ±1.0 Å^2.

3. Discussion

3.1 LaC_2 and ErC_2

For LaC_2, the refinement gives a slightly, but significantly, longer unit-cell dimension c than previously reported (*15, 16*) and a redetermined C–C bond length. For ErC_2, c is significantly longer than previously reported (*15, 17*), while the C–C bond, now more accurately determined, is possibly shorter. Since La and Er are both triply ionized, the slightly longer C–C bond in LaC_2 may be an indication of the increased f-orbital participation in M–C bonding as proposed earlier (*11*).

TABLE V

OBSERVED AND CALCULATED STRUCTURE FACTORS FOR CUBIC DICARBIDES

		Static model		Dynamic model	
	hkl	$\|F_o\|$	$\|F_c\|$	$\|F_o\|$	$\|F_c\|$
$Ce_{0.50}Er_{0.50}C_2$ (RT)	111	2.10	1.71	2.15	1.71
	200	5.73	5.73	5.88	5.88
	220	4.61	4.25	4.73	4.40
	311	0.00	0.01	0.00	0.01
	222	2.47	3.20	2.53	3.29
		(R = 0.100)		(R = 0.101)	
$Ce_{0.75}Lu_{0.25}C_2$ (RT)	111	1.91	1.91	1.97	1.93
	200	5.20	5.20	5.36	5.38
	220	3.74	3.70	3.86	3.86
	311	0.00	0.02	0.00	0.02
	222	2.68	2.69	2.76	2.76
		(R = 0.006)		(R = 0.005)	
$Ce_{0.50}Lu_{0.50}C_2$ (RT)	111	1.71	1.77	1.76	1.79
	200	5.58	5.58	5.74	5.74
	220	4.65	4.10	4.79	4.26
	311	0.00	0.02	0.00	0.01
	222	2.61	3.07	2.68	3.16
		(R = 0.076)		(R = 0.070)	
$Ce_{0.25}Lu_{0.75}C_2$ (RT)	111	1.07	1.56	1.09	1.58
	200	5.65	5.65	5.78	5.78
	220	4.66	4.06	4.76	4.19
	311	0.00	0.02	0.00	0.00
	222	2.87	2.95	2.94	3.03
		(R = 0.084)		(R = 0.079)	
$Ce_{0.75}Lu_{0.25}C_2$ (4.2 K)	111	2.02	1.98	2.07	2.00
	200	5.47	5.47	5.61	5.66
	220	[a]		[a]	
	311	0.00	0.03	0.00	0.02
	222	3.13	3.14	3.22	3.21
		(R = 0.006)		(R = 0.012)	
$Ce_{0.50}Lu_{0.50}C_2$ (4.2 K)	111	1.93	1.61	1.97	1.63
	200	5.67	5.72	5.80	5.80
	220	[a]		[a]	
	311	0.00	0.27	0.00	0.33
	222	2.92	2.92	2.99	2.99
		(R = 0.060)		(R = 0.066)	
$Ce_{0.25}Lu_{0.75}C_2$ (4.2 K)	111	1.64	1.63	1.69	1.63
	200	5.30	5.86	5.49	6.04
	220	5.27	4.37	5.46	4.58
	311	0.00	0.03	0.00	0.00
	222	2.97	3.29	3.08	3.47
		(R = 0.120)		(R = 0.120)	
$U_{0.50}Ce_{0.50}C_2$ (RT)	111	1.76	1.49	1.75	1.48
	200	5.16	5.21	5.14	5.23
	220	3.80	3.45	3.78	3.44
	311	0.00	0.01	0.00	0.01
	222	1.76	2.32	1.75	2.25
		(R = 0.098)		(R = 0.098)	

TABLE V—*Continued*

		Static model		Dynamic model	
	hkl	$\|F_o\|$	$\|F_c\|$	$\|F_o\|$	$\|F_c\|$
$U_{0.25}Ce_{0.75}C_2$ (RT)	111	1.65	1.65	1.69	1.66
	200	4.65	4.64	4.76	4.76
	220	3.34	2.89	3.42	2.98
	311	0.00	0.00	0.00	0.03
	222	1.38	1.83	1.42	1.86
		(R = 0.082)		(R = 0.083)	

Note. Each set of observed structure factors is scaled to the appropriate calculated set.

[a] For $Ce_{0.75}Lu_{0.25}C_2$ and $Ce_{0.50}Lu_{0.50}C_2$ at 4.2 K, the intensity of the 220 peaks could not be determined because of overlap with the 200 peak from the aluminum in the cryostat tail.

3.2 Cubic Dicarbides

One consequence of the lattice strain needed to form the cubic phase appears to be the broadening of the neutron diffraction peaks and the loss of the higher index peaks required for a complete profile analysis.

3.2.1. Unit cell parameters. For the Ce–Er and Ce–Lu structures, the room-temperature unit-cell parameters a (Table IV) show the variations expected from the sequence of ionic radii Ce $\gg$ Er > Lu. The cell of $Ce_{0.50}Er_{0.50}C_2$ is larger than that of $Ce_{0.50}Lu_{0.50}C_2$ by approximately the difference (0.03 Å) in the ionic radii of Er^{3+} and Lu^{3+}. The cells for the three Ce–Lu compounds decrease in size with increasing lutetium content.

At 4.2 K the cubic unit cell is retained but there is an anomaly in that the cells for $Ce_{0.75}Lu_{0.25}C_2$ and $Ce_{0.25}Lu_{0.75}C_2$ are marginally smaller than at room temperature, but that for $Ce_{0.50}Lu_{0.50}C_2$ is considerably larger, possibly as a result of a low-temperature phase-change. For the U–La and U–Ce structures, the unit-cell parameters do not change as steadily with composition as in the room-temperature Ce–Lu structures. Taking the longer of the two parameters for the 75% uranium structures, it appears that

TABLE VI

CARBON ATOM POSITIONAL PARAMETERS, ISOTROPIC THERMAL PARAMETERS AND C–C BOND LENGTHS FOR CUBIC DICARBIDES

	Static Model				Dynamic Model		
	x	B(Å^2)	C–C (Å) (uncorr)	C–C (Å) (corr)	x	B(Å^2)	C–C (Å)
$Ce_{0.50}Er_{0.50}C_2$ (RT)	0.053	5.1	1.05	1.29	0.054	4.2	1.07
$Ce_{0.75}Lu_{0.25}C_2$ (RT)	0.058	5.3	1.16	1.39	0.058	4.5	1.16
$Ce_{0.50}Lu_{0.50}C_2$ (RT)	0.055	4.9	1.08	1.31	0.055	4.1	1.08
$Ce_{0.25}Lu_{0.75}C_2$ (RT)	0.052	6.1	1.00	1.31	0.052	5.5	1.00
$Ce_{0.75}Lu_{0.25}C_2$ (4.2 K)	0.058	3.6	1.16	1.31	0.058	2.7	1.16
$Ce_{0.50}Lu_{0.50}C_2$ (4.2 K)	0.044	8.4	0.90	1.37	0.043	8.1	0.88
$Ce_{0.25}Lu_{0.75}C_2$ (4.2 K)	0.051	5.0	0.97	1.23	0.052	4.1	0.99
$U_{0.50}Ce_{0.50}C_2$ (RT)	0.052	7.9	0.96	1.38	0.052	7.9	0.96
$U_{0.25}Ce_{0.75}C_2$ (RT)	0.056	9.2	1.06	1.50	0.056	8.6	1.06

a for the U–La structures increases slightly with increasing lanthanum content (as expected from ionic radii considerations), but a for the U–Ce structures may show a minimum in the 50% metal composition region. For both $U_{0.50}Ce_{0.50}C_2$ and $U_{0.25}Ce_{0.75}C_2$, the unit-cell parameters are appreciably smaller, by comparison with the corresponding lanthanum structures, than would be expected from ionic radii differences. This may imply that the cerium is present as Ce^{4+}.

3.2.2. Structure factor calculations. Most of the structures show acceptable fits between observed and calculated structure factors (Table V) but without any significant difference between the static and the dynamic models. For the two uranium–lanthanum structures, $U_{0.50}La_{0.50}C_2$ and $U_{0.25}La_{0.75}C_2$, absence of a reasonable fit over the range of parameter values examined suggests either that the proposed structure is incorrect or that these two compositions are multiphase (but with closely similar cell dimensions) as found by SEM.

The unexpectedly high thermal parameters, together with the similarity of fit for the two models, suggests that the true structure may have C–C bonds aligned along the [111] directions, but with considerable thermal oscillatory vibration about the bond midpoint. A bond length correction using the "upper limit" model of Busing and Levy (*24*) would therefore seem appropriate for the C–C bond lengths in the "static" model. This produces C–C bond lengths mostly in the range 1.3–1.4 Å (Table VI), consistent with the presence of tetrapositive cations (although that for $U_{0.25}Ce_{0.75}C_2$ seems anomalously long). The corrected lengths are probably accurate only to about ±0.05 Å, and do not vary significantly with composition or temperature.

Acknowledgments

We thank Dr. R. Steadman for helpful advice and Dr. Margaret M. Rebbeck for the SEM measurements. We are grateful to the SRC/SERC for financial support to J.Y., for an equipment grant to I.J.M., and for access to neutron-beam facilities.

References

1. I. J. McColm, I. Colquhoun, and N. J. Clark, *J. Inorg. Nucl. Chem.* **34,** 3809 (1972).
2. I. J. McColm, T. A. Quigley, and N. J. Clark, *J. Inorg. Nucl. Chem.* **35,** 1931 (1973).
3. M. Atoji, *J. Chem. Phys.* **54,** 3514 (1971).
4. A. L. Bowman, N. H. Krikorian, G. P. Arnold, T. C. Wallace, and N. G. Nereson, *Acta Crystallogr., Sect. B* **24,** 459 (1968).
5. A. L. Bowman, G. P. Arnold, W. G. Witteman, T. C. Wallace, and N. G. Nereson, *Acta Crystallogr.* **21,** 670 (1966).
6. A. L. Bowman, N. H. Krikorian, G. P. Arnold, T. C. Wallace, and N. G. Nereson, *Acta Crystallogr., Sect. B* **24,** 1121 (1968).
7. I. J. McColm, "Ceramic Science for Materials Technologists," p. 274, Leonard Hill, Glasgow (1983).
8. I. R. Loe, I. J. McColm, and T. A. Quigley, *J. Less-Common Met.* **46,** 217 (1976).
9. D. W. Jones, I. J. McColm, R. Steadman, and J. Yerkess, *J. Solid State Chem.* **62,** 172 (1986).
10. D. W. Jones, I. J. McColm, R. Steadman, and J. Yerkess, *J. Solid State Chem.* **68,** 219 (1987).
11. I. J. McColm, *J. Less-Common Met.* **78,** 287 (1981).
12. N. J. Clark, R. Mountford, and I. J. McColm, *J. Inorg. Nucl. Chem.* **34,** 2729 (1972).
13. J. S. Anderson, N. J. Clark, and I. J. McColm, *J. Inorg. Nucl. Chem.* **30,** 105 (1968).
14. G. E. Bacon, *Acta Crystallogr., Sect A* **28,** 357 (1972).
15. F. H. Spedding, K. Gschneidner, and A. H. Daane, *J. Am. Chem. Soc.* **80,** 4499 (1958).
16. M. Atoji, *J. Chem. Phys.* **35,** 1950 (1961).
17. M. Atoji, *J. Chem. Phys.* **57,** 2410 (1972).
18. H. M. Rietveld, *J. Appl. Crystallogr.* **2,** 65 (1969).
19. A. W. Hewat, *J. Phys. C. Solid State Phys.* **6,** 2559 (1973).
20. D. W. Jones, I. J. McColm, R. Steadman, and J. Yerkess, *J. Solid State Chem.* **53,** 376 (1984).
21. A. K. Cheetham and J. C. Taylor, *J. Solid State Chem.* **21,** 253 (1977).
22. D. W. Jones, I. J. McColm, J. Yerkess, and N. J. Clark, *J. Solid State Chem.* **74,** 304 (1988).
23. A. W. Hewat, *Acta Crystallogr., Sect A* **35,** 248 (1979).
24. W. R. Busing and H. A. Levy, *Acta Crystallogr.* **17,** 142 (1964).
25. N. Elliott and J. Hastings, *Acta Crystallogr.* **14,** 1018 (1961).